Inorg. Chem. **2006**, *45*, 4448–4460

Iron Porphyrin–Cyclodextrin Supramolecular Complex as a Functional Model of Myoglobin in Aqueous Solution

Koji Kano,*,† Hiroaki Kitagishi,† Camille Dagallier,† Masahito Kodera,† Takashi Matsuo,§ Takashi Hayashi,§ Yoshio Hisaeda,‡ and Shun Hirota||

Department of Molecular Science and Technology, Faculty of Engineering, Doshisha University, Kyotanabe, Kyoto 610-0321, Japan, Division of Applied Chemistry, Graduate School of Engineering, Osaka University, Suita, Osaka 562-0014, Japan, Department of Chemistry and Biochemistry, Graduate School of Engineering, Kyushu University, Fukuoka 819-0395, Japan, and Department of Physical Chemistry, 21st Century COE Program, Kyoto Pharmaceutical University, Yamashina-ku, Kyoto 607-8414, Japan

Received January 23, 2006

The 1:1 inclusion complex of 5,10,15,20-tetrakis(4-sulfonatophenyl)porphinato iron(II) (Fe^{II}TPPS) and an O-methylated β-cyclodextrin dimer having a pyridine linker (**1**) binds dioxygen reversibly in aqueous solution. The O_2 adduct was very stable ($t_{1/2}$ = 30.1 h) at pH 7.0 and 25 °C. ESI-MS and NMR spectroscopic measurements and molecular mechanics (MM) calculations indicated the inclusion of the sulfonatophenyl groups at the 5- and 15-positions of Fe^{III}TPPS or Fe^{II}TPPS into two cyclodextrin moieties of **1** to form a supramolecular 1:1 complex (hemoCD1 for the Fe^{II}TPPS complex), whose iron center is completely covered by two cyclodextrin moieties. Equilibrium measurements and laser flash photolysis provided the affinities ($P_{1/2}^{O2}$ and $P_{1/2}^{CO}$) and rate constants for O_2 and CO binding of hemoCD1 (k_{on}^{O2}, k_{off}^{O2}, k_{on}^{CO}, and k_{off}^{CO}). The CO affinity relative to the O_2 affinity of hemoCD1 was abnormally high. Although resonance Raman spectra suggested weak back-bonding of $d_\pi(Fe) \rightarrow \pi^*(CO)$ and hence a weak CO–Fe bond, the CO adduct of hemoCD1 was very stable. The hydrophobic CO molecule dissociated from CO-hemoCD1 hardly breaks free from a shallow cleft in hemoCD1 surrounded by an aqueous bulk phase leading to fast rebinding of CO to hemoCD1. Isothermal titration calorimetry furnished the association constant (K^{O2}), $\Delta H°$, and $\Delta S°$ for O_2 association to be $(2.71 \pm 0.51) \times 10^4$ M^{-1}, -65.2 ± 4.4 kJ mol^{-1}, and -133.9 ± 16.1 J mol^{-1} K^{-1}, respectively. The autoxidation of oxy-hemoCD1 was accelerated by H^+ and OH^-. The inorganic anions also accelerated the autoxidation of oxy-hemoCD1. The O_2–Fe^{II} bond is equivalent to the $O_2^{\bullet-}$–Fe^{III} bond, which is attacked by the inorganic anions or the water molecule to produce met–hemoCD1 and a superoxide anion.

Introduction

Modeling the functions of hemoglobin (Hb) and myoglobin (Mb) in aqueous solution is very important not only to understand the mechanisms for dioxygen (O_2) transport and storage in biological systems[1] but also to develop new O_2-transport materials. A picket-fence porphyrin first prepared by Collman and co-workers is a typical Mb model, which possesses functions for protecting the formation of a μ-oxo dimer and a six-coordinate iron(II) porphyrin (B_2Fe^{II}Por, where B represents a base such as imidazole).[2] Following this, many model compounds have been designed and synthesized.[1,3] The fundamental concept of these model systems is almost the same as that of the picket-fence porphyrin. Although these elegantly designed Mb models have provided valuable information concerning O_2 binding to Fe^{II}Por, the serious limitation is solvent. Most models are effective only in absolute organic solvents, where a trace amount of water causes autoxidation of the O_2 adducts. Recently, the dendrimer-type Mb models were developed to investigate the effects of water on O_2 binding.[4,5] Zingg et

* To whom correspondence should be addressed. E-mail: kkano@mail.doshisha.ac.jp. Phone: 81-774-65-6624. Fax: 81-774-65-6845.
† Doshisha University.
§ Osaka University.
‡ Kyushu University.
|| Kyoto Pharmaceutical University.

(1) (a) Collman, J. P.; Boulatov, R.; Sunderland, C. J.; Fu, L. *Chem. Rev.* **2004**, *104*, 561−588. (b) Trayler, T. G. *Acc. Chem. Res.* **1981**, *14*, 102−109.
(2) (a) Collman, J. P.; Gagne, R. R.; Halbert, T. R.; Marchon, J.-C.; Reed, C. A. *J. Am. Chem. Soc.* **1973**, *95*, 7868−7870. (b) Collman, J. P. *Acc. Chem. Res.* **1977**, *10*, 265−272.
(3) Momenteau, M.; Reed, C. A. *Chem. Rev.* **1994**, *94*, 659−698.

10.1021/ic060137b CCC: $33.50 © 2006 American Chemical Society
Published on Web 05/02/2006

al. synthesized Fe^{II}Por dendrimers with polyoxyethylene chains.[5] These dendrimers are soluble in water, but do not form stable O_2 adducts even in water-saturated toluene. Quite recently, Collman et al. reported that a water-soluble picket-fence cobalt(II) porphyrin binds dioxygen in water, while a corresponding Fe(II) porphyrin does not form a dioxygen adduct.[6] The X-ray structures of Mb[7] and Hb[8] indicate that the prosthetic group, protoporphyrin IX, is located near the surface of the globin protein. Notwithstanding such a structure, autoxidation scarcely proceeds in biological systems.[9] Judging from the X-ray structural data, formation of an O_2 adduct in aqueous solution is expected to be achieved in a system where a base-coordinated Fe^{II}Por (B-Fe^{II}Por) is placed in a microscopically hydrophobic environment. Indeed, upon placing hydrophobic or amphiphilic B-Fe^{II}Pors in hydrophobic environments, such as liposomal membranes or albumin, relatively stable O_2 adducts are formed in aqueous media.[10−12] Recently, we prepared a supramolecular Mb functional model "hemoCD1" composed of an O-methylated β-cyclodextrin dimer with a pyridine linker (**1**) and 5,10,15,20-tetrakis(4-sulfonatophenyl)porphinato iron(II) (Fe^{II}TPPS) that binds O_2 reversibly in aqueous solution (Figure 1).[13] As shown in Figure 1, the central metal ion of Fe^{II}TPPS was assumed to be located at a hydrophobic cleft prepared by two O-methylated cyclodextrin moieties. Dimer **1** possesses the prerequisites of a globin functional model: a site to which Fe^{II}Por is bound through a noncovalent bond and a proximal base (pyridine) that can coordinate to Fe^{II}Por. HemoCD1 forms a very stable O_2 adduct (oxy-hemoCD1, half-life = 30.1 h in pH 7.0 phosphate buffer at 25 °C) and shows a moderate O_2 affinity ($P_{1/2}^{O2} = 17.5 \pm 1.7$ Torr).[13] Since hemoCD1 is a Mb functional model that works in aqueous solution, investigations using this model may provide valuable information on the factors that control the stability of the O_2−FePor complexes, factors such as water, inorganic anions, and pH.

We focused the present study on requirements for a Mb (Hb) functional model in aqueous solution, discrimination between O_2 and CO by hemoCD1, and the mechanism for autoxidation of oxy-hemoCD1. The results revealed the reasons why hemoCD1 acts as an excellent functional model for Mb and Hb that works in aqueous solution. The kinetics of O_2 and CO binding and the resonance Raman spectroscopy of CO-bound hemoCD1 suggested the mechanism for novel CO-selective binding of hemoCD1. The kinetics of autoxidation of oxy-hemoCD1 represented the mechanism for the autoxidation of oxy-hemoCD1 in aqueous solution involving nucleophilic attack of water or an inorganic anion to oxy-hemoCD1.

Experimental Section

Materials. Fe^{III}TPPS was prepared in the previous study.[14] Fe^{III}TPP was synthesized by an ordinary method.[15] Synthesis of the O-methylated β-cyclodextrin dimer **1** was described in the previous paper.[13] TMe-β-CD (Nacalai) and other chemicals were purchased and used as received. Water was purified using a Millipore Simpak 1. Pure O_2 (99.999%), pure N_2 (99.999%), and diluted CO (0.0909% CO in N_2) gases were purchased from Sumitomo Seika Chemicals. ^{13}CO (ICON, ^{13}C 99 atom %) was used for resonance Raman spectroscopic measurements.

Instruments. UV−vis spectra were taken using the Shimadzu UV-2100 and UV-2450 spectrophotometers with the thermostatic cell holders. The pH values were measured with a Horiba pH meter M-12. ESI-MS spectrum of met-hemoCD1 was recorded on a JEOL JMS-T100CS spectrometer using a negative mode at room temperature. The NMR spectrum of CO−hemoCD1 was recorded on a JEOL JNM-ECA500 spectrometer in D_2O (CEA, 99.9%) using sodium 3-trimethylsilyl[2,2,3,3-$^2H_4$]propionate (TSP, Aldrich) as an external standard. Raman scattering was excited at 413.1 nm with a Kr^+ laser (Spectra Physics, model 2060) and detected with a CCD detector (Princeton Instruments, PI-CCD) attached to a single polychromator (Ritsu Oyo Kogaku, DG-1000). Microcalorimetric measurements were carried out with a Microcal isothermal titration calorimeter VP−ITC. Kinetic measurements for ligand association of hemoCD1 were carried out with a laser flash photolysis system manufactured by Unisoku (Osaka, Japan) with a 5 ns pulse laser beam from a Q-switched Nd:YAG laser (Surelite I, Continuum). Mixed O_2 gases with various partial pressures in N_2 and mixed CO gases with various partial pressures in O_2 were prepared with a KOFLOC GM-4B gas mixing apparatus (Kyoto, Japan).

Preparation of Stock Solution of Oxy-hemoCD1. An excess amount of $Na_2S_2O_4$ (1 mg, 5.7×10^{-6} mol) was added to the 1 mL of the met-hemoCD1 solution ([Fe^{III}TPPS] = 3.0×10^{-4} M, [**1**] = 3.6×10^{-4} M in 0.05 M phosphate buffer at pH 7.0). The resulting solution was charged to a Sephadex G-25 column (16×25 mm^2, superfine, HiTrap desalting column, Amersham Biosciences) and eluted with pure water under aerobic conditions to remove excess $Na_2S_2O_4$ and its oxidized derivatives. During column chromatography, deoxy-hemoCD1 changed to oxy-hemoCD1. The purified oxy-hemoCD1 solution was stored in a refrigerator (4 −5 °C) and used within 2 days. The concentration of oxy-hemoCD1 was determined by using the absorption coefficient (ϵ_{max} = 110 400 M^{-1} cm^{-1}) at 423 nm.[13]

(4) Jiang, D.-L.; Aida, T. *Chem. Commun*. **1996**, 1523−1524.
(5) Zingg, A.; Felber, B.; Gramlich, V.; Fu, L.; Collman, J. P.; Diederich, F. *Helv. Chem. Acta* **2002**, *85*, 333−351.
(6) Collman, J. P.; Yan, Y.-L.; Eberspacher, T.; Xie, X.; Solomon, E. I. *Inorg. Chem.* **2005**, *44*, 9628−9630.
(7) (a) Kendrew, J. C.; Bodo, G.; Dintzis, H. M.; Parrish, R. G.; Wyckoff, H.; Phillips, D. C. *Nature* **1958**, *181*, 662−666. (b) Kendrew, J. C.; Dickerson, R. E.; Strandberg, B. E.; Hart, R. G.; Davis, D. R.; Phillips, D. C.; Shore, V. C. *Nature* **1960**, *185*, 422−427. (c) Kendrew, J. C. *Science* **1963**, *139*, 1259−1266.
(8) (a) Perutz, M. F.; Rossmann, M. G.; Cullis, A. F.; Muirhead, H.; Will, G.; North, A. C. T. *Nature* **1960**, *185*, 416−422. (b) Cullis, A. F.; Muirhead, H.; Perutz, M. F.; Rossmann, M. G.; North, A. C. T. *Proc. R. Soc. London, Ser. A* **1962**, *265*, 161−187. (c) Perutz, M. F. *Science* **1963**, *140*, 863−869.
(9) (a) Shikama, K. *Chem. Rev.* **1998**, *98*, 1357−1373. (b) Shikama, K. *Coord. Chem. Rev.* **1988**, *83*, 73−91.
(10) (a) Tsuchida, E.; Nishide, H.; Yuasa, M.; Hasegawa, E.; Matsushita, Y. *J. Chem. Soc., Dalton Trans.* **1984**, 1147−1151. (b) Komatsu, T.; Moritake, M.; Nakagawa, A.; Tsuchida, E. *Chem.−Eur. J.* **2002**, 8, 5469−5480.
(11) (a) Komatsu, T.; Ohmichi, N.; Zunszain, P. A.; Curry, S.; Tsuchida, E. *J. Am. Chem. Soc.* **2004**, *126*, 14304−14305. (b) Nakagawa, A.; Ohmichi, N.; Komatsu, T.; Tsuchida, E. *Org. Biomol. Chem.* **2004**, *2*, 3108−3112.
(12) Tsuchida, E. *Artificial Red Cells*; John Wiley & Sons: New York, 1995.
(13) Kano, K.; Kitagishi, H.; Kodera, M.; Hirota, S. *Angew. Chem., Int. Ed.* **2005**, *44*, 435−438.
(14) Kano, K.; Kitagishi, H.; Tamura, S.; Yamada, A. *J. Am. Chem. Soc.* **2004**, *126*, 15202−15210.
(15) Fleischer, E. B.; Palmer, J. M.; Srivastava, T. S.; Chatterjee, A. *J. Am. Chem. Soc.* **1971**, *93*, 3162−3167.

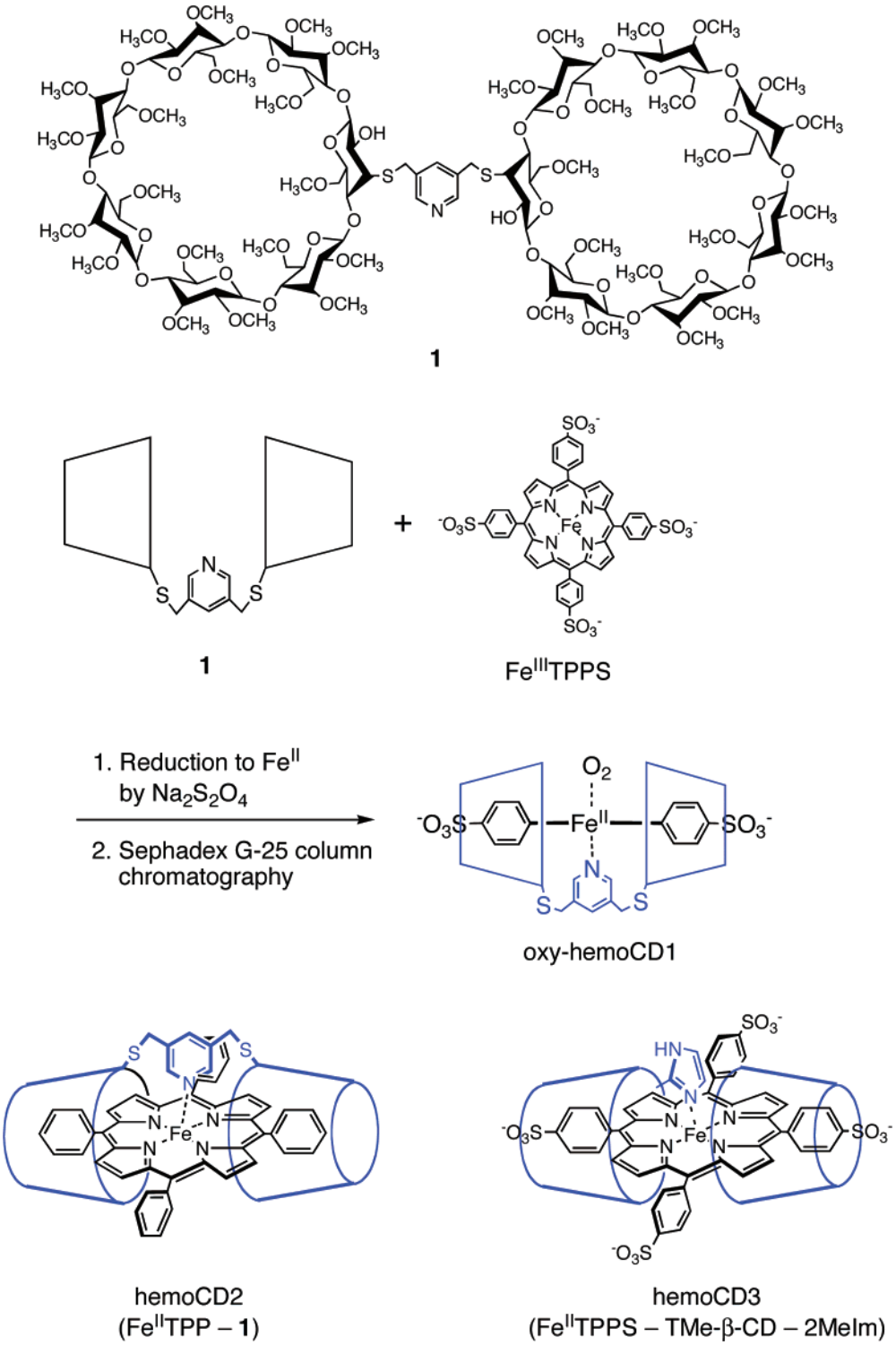

Figure 1. Formation of oxy-hemoCD1 from O-methylated β-cyclodextrin dimer **1** and Fe^{III}TPPS and other Fe^{II}Por-cyclodextrin systems used in this study.

Preparation of HemoCD2 Solution. Fe^{III}TPP (2.5 mg, 2.8×10^{-6} mol) and **1** (10 mg, 3.4×10^{-6} mol) were dissolved in 6 mL of a mixed solvent of methanol and water (5/1 (v/v)). Methanol was evaporated under reduced pressure at an ambient temperature. After the methanol was removed, no precipitation was formed, indicating that water-insoluble Fe^{III}TPP was solubilized in water by **1**. The remaining aqueous solution was deaerated by freeze−pump−thaw cycles (4 times), and the solution was transferred to a glovebox filled with Ar. The Fe^{III}TPP−**1** complex was reduced to the Fe^{II} complex by adding an excess amount of $Na_2S_2O_4$ (1.0 mg, 5.7×10^{-6} mol). A deoxygenated 0.05 M phosphate buffer solution (pH 7.0) was added to the solution up to 5 mL. The solution was transferred to a glass tube sealed with a silicone cap. For UV−vis spectral measurement, 25 μL of the stock solution was diluted to 3 mL by deoxygenated 0.05 M phosphate buffer (pH 7.0) in a quartz cell (10 mm optical length) with a screw cap. The final concentrations of Fe^{II}TPP and **1** were 4.7×10^{-6} and 5.6×10^{-6} M, respectively.

Raman Measurements. The excitation laser beam was focused to about 50 μm at the sample point, and the laser power was adjusted to 12 mW. A spinning cell (3000 rpm) was used to avoid photo dissociation of CO. All measurements were carried out at room temperature. Raman shifts were calibrated with acetone and toluene for the low-frequency region and with acetone and acetonitrile for the high-frequency region.

Determination of O_2 and CO Affinities. The O_2-N_2 mixed gas with a certain partial pressure was bubbled into the phosphate buffer solution (0.05 M, pH 7.0, 3 mL) in a quartz cell (10 mm optical length). After the gas was bubbled for at least 15 min, 50 μL of the stock solution of oxy-hemoCD1 was added quickly, and the bubbling was continued for additional 3 min. The UV−vis spectrum of the resulting solution was recorded at 25 ± 0.1 °C. The $P_{1/2}^{O2}$ value was determined spectroscopically according to the procedure described in the literature.[5,16] The *M* value was evaluated by measuring the absorption spectral changes of oxy-hemoCD1 which was placed under the $CO/O_2/N_2$ mixed gases with various partial pressures of CO.

Kinetic Measurements for O_2 and CO Binding. The solutions of oxy-hemoCD1 were prepared by the same procedures as equilibrium measurements described above. The concentration of oxy-hemoCD1 was 1×10^{-5} M in 0.05 M phosphate buffer at pH 7.0. The solution of CO-hemoCD1 was prepared by adding an excess amount of $Na_2S_2O_4$ (10 equiv) to the solution of met-hemoCD1 (1×10^{-5} M) in 0.05 M phosphate buffer at pH 7.0 under CO atmosphere. Rebinding of O_2 and CO was monitored by following the changes in the absorbances at 437 nm for oxy-hemoCD1 and at 434 nm for CO-hemoCD1 after excitation by a laser flash (λ_{ex} = 532 nm, 5 ns pulse) at pH 7.0 and 25 °C. The photolyses were carried out under air and CO atmospheres for the O_2 and CO binding measurements, respectively. The pseudo-first-order rate constants for O_2 and CO association were determined by curve fitting analysis using the nonlinear least-squares method.

Calorimetric Measurement. One milliliter of the deoxygenated solution of met-hemoCD1 ($[Fe^{III}TPPS] = 4.43 \times 10^{-3}$ M, [**1**] = 5.31×10^{-3} M, 0.05 M phosphate buffer at pH 7.0) in a glass tube sealed with a silicone cap was reduced by a slightly excess amount of $Na_2S_2O_4$ (0.8 mg, 4.60×10^{-6} mol, 1.05 equiv) under N_2 atmosphere to obtain hemoCD1. The inside of a syringe of the ITC instrument was filled with pure N_2 before use. The deoxy-hemoCD1 solution (250 μL) was transferred to the syringe, and the 25 aliquots (10 μL each) were added into the N_2- and air-saturated buffers (0.05 M phosphate, pH 7.0) to measure the heat of dilution and the heat of complexation, respectively. The titration curve thus obtained was analyzed using the *one-site model* in the ORIGIN software program. We employed 2.64×10^{-4} M as the concentration of O_2 in phosphate buffer.[17]

Kinetic Measurements for Autoxidation. In all cases, 50 μL of the stock solution of oxy-hemoCD1 was added into 3 mL of the appropriate solution in a quartz cell (10 mm optical length). The concentrations of oxy-hemoCD1 were $5-7 \times 10^{-6}$ M. The rate of autoxidation of oxy-hemoCD1 was measured by monitoring the changes in absorbance of oxy-hemoCD1. The reaction was followed until more than 85% of oxy-hemoCD1 was converted to met-hemoCD1. The pH values of the solution were carefully checked before and after the measurement. The time course of the absorbance change at λ_{max} of the Soret band was analyzed by pseudo-first-order kinetics to obtain an apparent rate constant for the autoxidation (k_{obs}).

Results

Structure of HemoCD1. Heptakis(2,3,6-tri-*O*-methyl)-β-cyclodextrin (TMe-β-CD) is known to form extremely stable 2:1 inclusion complexes with 5,10,15,20-tetrakis(4-sulfonatophenyl)porphyrin (TPPS) and its Fe^{III} complex (Fe^{III}TPPS) in aqueous solution.[14,18,19] The formation of such unusually stable complexes is interpreted in terms of induced-fit-type inclusion of TPPS and Fe^{III}TPPS by TMe-β-CD.[18,19] Previously, the novel nature of per-O-methylated β-cyclodextrin was applied to form the inclusion complex of Fe(TPPS) and the O-methylated β-cyclodextrin dimer **1** (Figure 1).[13] The sharp saturation of the absorbance changes in the UV−vis spectroscopic titration curve suggests the formation of a very stable 1:1 complex of Fe^{III}TPPS and **1**.[13] In the present study, the formation of the 1:1 complex of Fe^{III}TPPS and **1** was definitely confirmed by means of ESI-MS (negative mode) spectroscopy. Two peaks were observed at *m*/*z* 1307 and 985 that correspond to $[Fe^{III}TPPS\text{-}\mathbf{1}]^{3-}$ (molecular weight 3923) and $[Fe^{III}(OH)TPPS\text{-}\mathbf{1}]^{4-}$ (molecular weight 3940), respectively. The binding constant (*K*) for the $Fe^{III}TPPS-\mathbf{1}$ complex was too large to be determined accurately from a direct titration experiment.

Previously, we found that dioxygen in oxy-hemoCD1 is easily replaced by carbon monoxide to afford CO-hemoCD1.[13] Diamagnetic CO-hemoCD1 is so stable that this compound is suitable as a model for deducing the structure of hemoCD1 from detailed analysis of its NMR spectral data. Although the detailed results are not shown herein,[20] the point of the NMR spectrum of CO-hemoCD1 is the six signals from the OCH_3 groups at the 2- and 3-positions of the dimer **1** observed at 1.5−3.3 ppm. The high-field shifts of the signals resulting from the secondary OCH_3 groups suggest the inclusion of the sulfonatophenyl groups of Fe^{II}TPPS into the cyclodextrin cavities of **1**. The fact that only six types of secondary OCH_3 groups are measured at the higher-magnetic fields definitely indicates the formation of the inclusion complex taking a symmetrical structure. If the inclusion complex has an asymmetrical structure, the signals from the secondary OCH_3 groups should become more complex because dimer **1** has 12 secondary OCH_3 groups. On the basis of these NMR data, we can deduce the structure of oxy-hemoCD1 as shown in Figure 1. Such a symmetrical structure of oxy-hemoCD1 was also supported by the molecular mechanics (MM) calculations (vide infra).

O_2 Binding of Mb Functional Models. In the present work, the $Fe^{III}TPPS-\mathbf{1}$ complex (met-hemoCD1) in aqueous solution was reduced using an excess amount of $Na_2S_2O_4$ to

(16) Collman, J. P.; Zhang, X.; Wong, K.; Brauman, J. I. *J. Am. Chem. Soc.* **1994**, *116*, 6245−6251.
(17) Wilhelm, E.; Battino, R.; Wilcock, R. J. *Chem. Rev.* **1977**, *77*, 219−262.
(18) Kano, K.; Nishiyabu, R.; Asada, T.; Kuroda, Y. *J. Am. Chem. Soc.* **2002**, *124*, 9937−9944.
(19) Kano, K.; Nishiyabu, R.; Doi, R. *J. Org. Chem.* **2005**, *70*, 3667−3673.
(20) Kano, K.; Kitagishi, H.; Tanaka, S. *J. Inclusion Phenom. Macrocyclic Chem*. **2006**, In press.

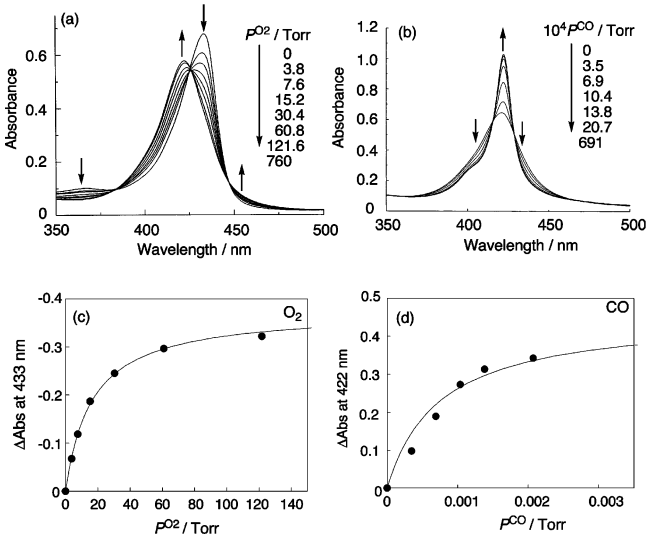

Figure 2. UV−vis spectral changes of hemoCD1 (5×10^{-6} M) as a function of the O_2 partial pressure (P^{O2}) in N_2 (a) and of oxy-hemoCD1 (5×10^{-6} M) as a function of the CO partial pressure (P^{CO}) in O_2-N_2 (b) in 0.05 M phosphate buffer at pH 7.0 and 25 °C and the equilibrium curves for O_2 binding to deoxy-hemoCD1 (c) and for CO binding to oxy-hemoCD1 (d). The solid lines in c and d are the theoretical curves for determining $P^L_{1/2}$ from the following equation: $\Delta Abs = ([hemoCD1]_t \Delta\epsilon P^L)/(P^L_{1/2} + P^L)$ where ΔAbs is the absorbance change of hemoCD1 (433 nm) or CO-hemoCD1 (422 nm) at a partial pressure (P^L) of O_2 or CO. The extinction coefficients (ϵ) of oxy-hemoCD1 and CO-hemoCD1 were determined from the absorption spectra under the O_2 and CO atmospheres (760 Torr), respectively.

yield the Fe^{II}TPPS−**1** complex (hemoCD1) under aerobic conditions, and the resulting solution was passed through a Sephadex G-25 column to remove excess $Na_2S_2O_4$ and its oxidized derivatives. During this treatment under aerobic conditions, the color of the reaction mixture changed from dull red to bloody red, indicating the formation of the O_2 adduct of hemoCD1 (oxy-hemoCD1).[21] The absorption spectrum of the resulting solution suggested quantitative formation of oxy-hemoCD1 (ϵ_{max} at 423 nm = 110 400 M^{-1} cm^{-1}). HemoCD1 captures O_2 from the air during the column chromatographic treatment. Oxy-hemoCD1 is so stable (vide infra) that the stock solution of oxy-hemoCD1 stored in a refrigerator (4−5 °C) can be used for several days. Dioxygen is easily removed from oxy-hemoCD1 to yield deoxy-hemoCD1 by bubbling nitrogen (N_2) gas into the oxy-hemoCD1 solution.[13] From the results shown in Figure 2a, the $P^{O2}_{1/2}$ value (the O_2 affinity) of hemoCD1 thus purified was determined to be 16.9 ± 1.8 Torr, which is in good agreement with the previous determination (17.5 ± 1.7 Torr).[13] $P^{O2}_{1/2}$ represents the partial dioxygen pressure at which half of the Fe^{II}Por molecules are coordinated by O_2.

In place of water-soluble Fe^{III}TPPS, Fe^{III}TPP (TPP = 5,10,15,20-tetraphenylporphyrin) was used as a hydrophobic Fe^{III}Por. Hydrophobic Fe^{III}TPP could be solubilized in aqueous solution by **1** (see Experimental Section). The experimental procedures were somewhat different from those employed for hemoCD1 because of the more labile nature of the O_2 adduct of the Fe^{II}TPP−**1** complex (oxy-hemoCD2). The Fe^{III}TPP−**1** complex (met-hemoCD2) in Ar-saturated phosphate buffer at pH 7.0 was reduced by 2 equiv of $Na_2S_2O_4$ to yield an Fe^{II}TPP−**1** complex (hemoCD2), which was aerated for 20 min. The absorption maximum of the O_2 adduct thus obtained was observed at 421 nm (SI Figure 1). Introducing CO gas into the O_2 adduct solution caused sharpening and enlargement of the spectrum (λ_{max} = 421 nm), indicating the formation of CO-bound hemoCD2. The O_2 affinity of hemoCD2 ($P^{O2}_{1/2}$ = 16.1 Torr) was almost the same as that of hemoCD1 (16.9 Torr), while the half-life of oxy-hemoCD2 ($t_{1/2}$ = 3.0 h) was much shorter than that of hemoCD1 (30.1 h) (SI Figure 2).

It has been known that 2-methylimidazole (2MeIm) forms a five-coordinate Fe^{II}Por (2MeIm−Fe^{II}Por) in organic solvents.[22] An intermolecular 2:1 complex of TMe-β-CD and Fe^{II}TPPS whose Fe^{II} was coordinated by 2MeIm was employed as a more convenient Mb model (Figure 1). Formation of the five-coordinate 2MeIm−Fe^{II}TPPS−(TMe-β-CD)$_2$ complex (hemoCD3) was confirmed by means of ^{1}H NMR spectroscopy (SI Figure 3). However, no O_2 adduct was formed upon introduction of the O_2 gas into the aqueous hemoCD3 solution, while immediate autoxidation took place. The formation of a CO adduct of hemoCD3 was verified by means of UV−vis spectroscopy. The methyl group of 2MeIm might expand the cleft formed by the two O-methylated β-cyclodextrin moieties, thus resulting in easy penetration of the water molecule into the cleft that causes the autoxidation of oxy-hemoCD3.

Affinities of HemoCD1 for Binding O_2 and CO. It has been known that the O_2 affinities of native Mb and Hb relative to their respective CO affinities are higher than those of the model systems in toluene (Table 1). The relative affinity is represented by the M value obtained from the O_2 ($P^{O2}_{1/2}$) and CO affinities ($P^{CO}_{1/2}$)

$$P^{O2}_{1/2} = \{[\text{deoxy-hemoCD1}]P^{O2}\}/[\text{oxy-hemoCD1}] \quad (1)$$

$$P^{CO}_{1/2} = \{[\text{deoxy-hemoCD1}]P^{CO}\}/[\text{CO-hemoCD1}] \quad (2)$$

$$M = P^{O2}_{1/2}/P^{CO}_{1/2} = \{[\text{CO-hemoCD1}]P^{O2}\}/\{[\text{oxy-hemoCD1}]P^{CO}\} \quad (3)$$

The $P^{O2}_{1/2}$ value for hemoCD1 determined from the results shown in Figure 2 was 16.9 ± 1.8 Torr. After the UV−vis spectra were measured to determine $P^{O2}_{1/2}$, the UV−vis spectral changes were taken further after the oxy-hemoCD1 solution was exposed to the atmospheres containing CO at various partial pressures in the mixed gases of O_2 and N_2 (Figure 2b). From the titration curve, the partial CO pressure (P^{CO}) at which [CO-hemoCD1] = [oxy-hemoCD1] was determined to be $(6.9 \pm 0.6) \times 10^{-4}$ Torr. At this point, P^{O2} was 759.24 Torr (the value was corrected by considering the partial pressure of the N_2 gas for diluting CO). Then the M value of hemoCD1 in 0.05 M phosphate buffer at pH 7.0

(21) The formation of oxy-hemoCD1 has been verified by measuring UV−vis, ^{1}H NMR, and resonance Raman spectra.[13]

(22) Collman, J. P.; Reed, C. A. *J. Am. Chem. Soc.* **1973**, *95*, 2048−2049.

Table 1. Kinetic Data for Binding of O_2 and CO in Biological and Model Systems

system	$P_{1/2}^{O2}$ (Torr)	k_{on}^{O2} (M^{-1} s^{-1})	k_{off}^{O2} (s^{-1})	$P_{1/2}^{CO}$ (Torr)	k_{on}^{CO} (M^{-1} s^{-1})	k_{off}^{CO} (s^{-1})	M	ref
Mb (sperm whale)	0.54[a]	1.7×10^7	15	0.029[a]	5.1×10^5	0.019	18.6	23
Mb (human)	0.69[a]	1.9×10^7	22	0.023[a]	7.6×10^5	0.022	30	23
Hb (human, R state)	0.22	3.3×10^7	13.1	1.3×10^{-3}	4.6×10^6	9×10^{-3}	150	1a
$FePiv_35CIm$[b]	0.58	4.3×10^8	2.9×10^3	2.2×10^{-5}	3.6×10^7	7.8×10^{-3}	26 600	24
Fe(PF3CUIm)[b]	1.26	2.6×10^8	3.9×10^3	4.9×10^{-5}	2.9×10^7	1.4×10^{-2}	26 000	25
Fe(PF3CUPy)[b]	52.2	3.0×10^8	1.9×10^5	6.4×10^{-4}	4.8×10^7	0.33	76 000	25
TCP−IM[b]	1.3	4.0×10^7	2.0×10^3	1.1×10^{-3}	2.1×10^7	0.23	1180	26
TCP−PY[b]	9.4	2.7×10^7	2.5×10^3	1.7×10^{-2}	1.6×10^7	3.2	550	26
hemoCD1	16.9	4.7×10^7	1.3×10^3	1.5×10^{-5}	1.3×10^7	2.5×10^{-4}	1.1×10^6	this work

[a] These values were calculated from K values reported in ref 23. [b] $FePiv_35CIm$ = *meso*-5α,10α,15α-tris(*o*-pivalamidophenyl)-20*β*-{*o*-[5-(*N*-imidazolyl)valeramido]phenyl}-porphyrinatoiron, Fe(PF3CUIm) = *meso*-5α,10α,15α-tris(*o*-pivalamidophenyl)-20*β*-{*o*-{[3-(*N*-imidazolyl)propyl] ureido}phenyl}porphyrinatoiron, Fe(PF3CUPy) = *meso*-5α,10α,15α-tris(*o*-pivalamidophenyl)-20*β*-{*o*-{[3-(3-pyridyl)propyl]ureido}phenyl}porphyrinatoiron. TCP−IM and TCP−PY = iron(II) complexes of tetraphenylporphyrin derivative whose 2′- and 6′-positions of the phenyl groups are substituted by the naphthyl derivatives (registry number: 7439-89-6). The experiments of these model compounds were carried out in absolute toluene. The k_{off} values for the present systems were calculated from k_{on} and $P_{1/2}$ values, while the k_{off} values for the biological systems were determined from ligand replacement reactions. Therefore, direct comparisons of these k_{off} values might be somewhat problematic.

and 25 °C was evaluated to be 1.1×10^6. Equation 3 gave a $P_{1/2}^{CO}$ value of 1.5×10^{-5} Torr.

Kinetics of HemoCD1 for Binding O_2 and CO. The rate constants for association (k_{on}) of O_2 and CO with CO-hemoCD1 were determined from laser flash photolysis (SI Figure 4).[26,27] The reaction pathways can be written as follows

$$\text{L−hemoCD1} \xrightarrow{h\nu} \text{deoxy-hemoCD1} + \text{L} \qquad (4)$$

$$\text{deoxy-hemoCD1} + \text{L} \underset{k_{off}^{L}}{\overset{k_{on}^{L}}{\rightleftharpoons}} \text{L−hemoCD1} \qquad (5)$$

$$k_{obs}^{L} = k_{on}^{L}[\text{L}] + k_{off}^{L} \qquad (6)$$

where L represents the ligand such as O_2 or CO. The k_{obs}^{O2} values were measured at various partial pressures of O_2, and the k_{on}^{O2} value (4.7×10^7 M^{-1} s^{-1}) was determined from the slope of a linear relation between k_{obs}^{O2} and [O_2] (SI Figure 5). The k_{off}^{O2} value was calculated from eq 7[25] where C is the

$$K^{O2} = (CP_{1/2}^{O2})^{-1} = k_{on}^{O2}/k_{off}^{O2} \qquad (7)$$

solubility of O_2 in water at 25 °C ($C = 1.67 \times 10^{-6}$ M Torr^{-1}).[17] As shown in Table 1, the k_{on}^{O2} and k_{off}^{O2} values determined are 4.7×10^7 M^{-1} s^{-1} and 1.3×10^3 s^{-1}, respectively. The $P_{1/2}^{CO}$ value is so small that the k_{obs}^{CO} value is approximately equal to k_{on}^{CO}[CO]. The k_{off}^{CO} value was calculated from an equation corresponding to eq 7 ($C = 1.26 \times 10^{-6}$ M Torr^{-1}).[17] It can be concluded that the abnormally large M value (1.1×10^6) for the hemoCD1 system in aqueous solution is the result of the very slow dissociation of CO from CO-hemoCD1. Since both k_{off}^{O2} and k_{off}^{CO} were calculated using the $P_{1/2}^{O2}$ and $P_{1/2}^{CO}$ values, respectively, these k_{off} values were apparent.

Resonance Raman Spectrum of CO−hemoCD1. Resonance Raman spectra of CO-hemoCD1 were measured to determine the structure of this complex and to study the environmental effect of the present system. The resonance Raman spectra of CO-hemoCD1 in the lower- and higher-frequency regions are shown in Figure 3. Assignment of the Raman peaks was carried out by observing isotopic shifts using ^{13}CO. It is known that the Fe−CO stretching (ν_{Fe-CO}), Fe−C−O bending (δ_{FeCO}), and C−O stretching (ν_{CO}) bands of CO−Mb are observed at 507, 578, and 1951 cm^{-1}, respectively.[28] In the case of CO-hemoCD1, the ν_{Fe-CO} and ν_{CO} bands were observed at 480 and 1987 cm^{-1}, respectively. No Fe−C−O bending mode was detected around 570−580 cm^{-1}, indicating that the CO molecule adopts a linear geometry in the CO complex of hemoCD1. Compared with the reported frequencies for the ν_{Fe-CO} and ν_{CO} bands of hemoproteins and their model systems with nitrogenous axial base ligands, the ν_{Fe-CO} and ν_{CO} bands of CO-hemoCD1 appear at significantly lower and higher frequencies, respectively. The results suggest very weak back-bonding of d_π(Fe) → π^*(CO) in CO−hemoCD1 (see Discussion).

Calorimetric Titration. Isothermal titration calorimetry (ITC) is the best method to obtain accurate thermodynamic parameters for complexation because this method measures evolved heat ($\Delta H°$) directly. In the most cases, the thermodynamic parameters for O_2 coordination to Mb, Hb, and their model compounds have been evaluated from van't Hoff plots (eq 8).[26,29] Equation 8 is a special equation that correlates $P_{1/2}^{O2}$ with $\Delta H°$ and $\Delta S'$. A more general equation is

$$\ln(P_{1/2}^{O2}) = \Delta G'/(RT) = \Delta H°/(RT) - \Delta S'/R \qquad (8)$$

represented in eq 9. From eq 7, it is clear that $\Delta G'$ and $\Delta S'$

(23) Springer, B. A.; Sligar, S. G.; Olson, J. S.; Phillips, G. N., Jr. *Chem. Rev.* **1994**, *94*, 699−714.

(24) Collman, J. P.; Brauman, J. I.; Iverson, B. L.; Sessler, J. L.; Morris, R. M.; Gibson, Q. H. *J. Am. Chem. Soc.* **1983**, *105*, 3052−3064.

(25) Collman, J. P.; Brauman, J. I.; Doxsee, K. M.; Sessler, J. L.; Morris, R. M.; Gibson, Q. H. *Inorg. Chem.* **1983**, *22*, 1427−1432.

(26) Tani, F.; Matsu-ura, M.; Ariyama, K.; Setoyama, T.; Shimada, T.; Kobayashi, S.; Hayashi, T.; Matsuo, T.; Hisaeda, Y.; Naruta, Y. *Chem.−Eur. J.* **2003**, *9*, 862−870.

(27) (a) Matsuo, T.; Dejima, H.; Hirota, S.; Murata, D.; Sato, H.; Ikegami, T.; Hori, H.; Hisaeda, Y.; Hayashi, T. *J. Am. Chem. Soc.* **2004**, *126*, 16007−16017. (b) Sato, H.; Watanabe, M.; Hisaeda, Y.; Hayashi, T. *J. Am. Chem. Soc.* **2005**, *127*, 56−57.

(28) Kitagawa, T.; Hirota, S. In *Handbook of Vibrational Spectroscopy*; Chalmers, J. M., Griffiths, P. R., Ed.; John Wiley & Sons: Chichester, U.K., 2002; pp 1−21.

(29) (a) Imai, K.; Yonetani, T. *J. Biol. Chem.* **1975**, *250*, 7093−7098. (b) Wang, M.-Y. R.; Hoffman, B. M.; Shire, S. J.; Gurd, F. R. N. *J. Am. Chem. Soc.* **1979**, *101*, 7394−7397. (c) Collman, J. P.; Brauman, J. I.; Suslick, K. S. *J. Am. Chem. Soc.* **1975**, *97*, 7185−7186.

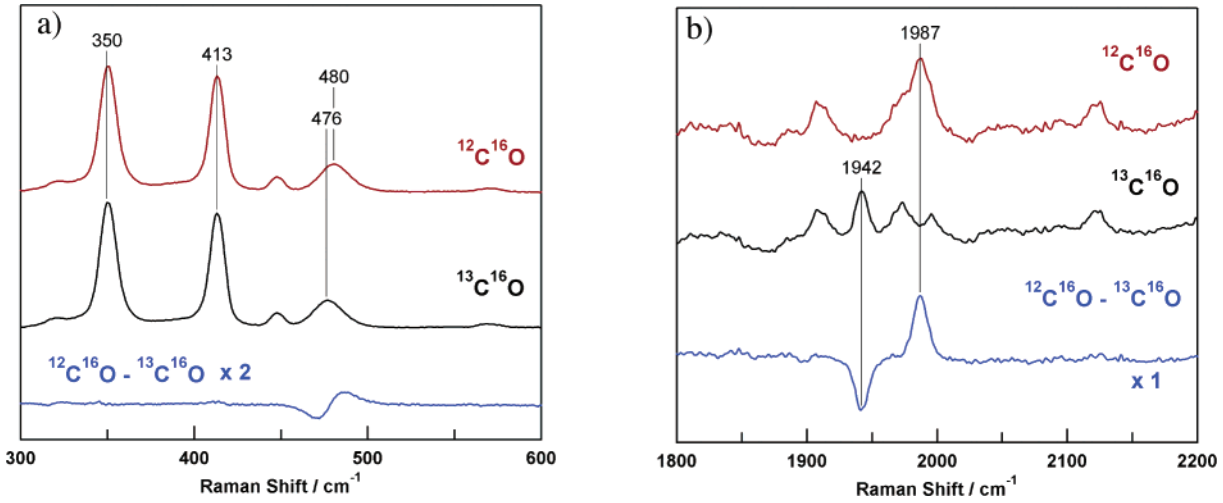

Figure 3. Resonance Raman spectra in the 300−600 cm^{-1} (Fe−CO stretching, ν_{Fe-CO}) (a) and 1800−2200 cm^{-1} regions (C−O stretching, ν_{CO}) (b) of the $^{12}C^{16}O$ and $^{13}C^{16}O$ adducts of hemoCD1 (5×10^{-5} M) in 0.05 M phosphate buffer at pH 7.0 and room temperature and their differential spectra. The sample was irradiated by a laser light of 413.1 nm at 12 mW power.

Table 2. Thermodynamic Data for O_2 Association in HemoCD1 and Other Systems

system	$\Delta H°$ (kJ mol^{-1})	$\Delta S°$ (J mol^{-1} K^{-1})	$\Delta G°$ (kJ mol^{-1})	K^{O2} (M^{-1})	ref
Hb (human)	−52.3	(−77.2) [a]	(−29.3) [a]	(1.4×10^5)[b]	29a
Mb (sperm whale)	−79.9	(−153.0) [a]	(−34.3) [a]	(1.0×10^6)[b]	29b
Mb (horse heart)	−87.8	(−182.3) [a]	(−33.5)[a]	(7.5×10^5)[b]	29b
TCP−IM[c]	−53.6	(−82.0) [a]	(−29.2) [a]	(1.3×10^5)[b]	26
TCP−PY[c]	−51.0	(−90.3) [a]	(−24.1) [a]	(1.7×10^4)[b]	26
Fe(TpivPP)(1-MeIm)[d]	−65.3				29c
HemoCD1	−65.2 ± 4.4	−134 ± 16	−25.3 ± 0.6	$(2.7 \pm 0.5) \times 10^4$	this work

[a] The $\Delta S°$ and $\Delta G°$ values in parentheses were evaluated from the original $\Delta S'$ values using eqs 7−9. For calculation, 1.67×10^{-6} and 6.97×10^{-6} M Torr^{-1} were used as the solubility of O_2 in water and toluene at 25 °C, respectively. [b] The K^{O2} values in parentheses were calculated using eq 9. [c] The experiments were carried out in absolute toluene. [d] The measurement was carried out in solid state. Fe(TpivPP)(1-MeIm) is a picket-fence Fe^{II}Por having the pivalamidophenyl groups whose Fe^{II} is coordinated by 1-methylimidazole.

in eq 8 differ from $\Delta G°$ and $\Delta S°$, respectively, in eq 9. In

$$-\ln K^{O2} = \Delta G°/(RT) = \Delta H°/(RT) - \Delta S°/R \qquad (9)$$

the present study, the association constant (K^{O2}) and the enthalpy change ($\Delta H°$) for the binding of O_2 to hemoCD1 were directly measured by means of ITC, and the entropy change ($\Delta S°$) was calculated. The titration curve (SI Figure 6) indicates the formation of the 1:1 complex of O_2 and hemoCD1 and its analysis gave the K^{O2} value of $(2.71 \pm 0.51) \times 10^4$ M^{-1}. The K^{O2} value determined is consistent with that calculated from $P_{1/2}^{O2}$ ($(3.54 \pm 0.42) \times 10^4$ M^{-1}) using eq 7. The thermodynamic parameters obtained are summarized in Table 2. Dioxygen association with hemoCD1 is an enthalpically favorable and entropically unfavorable process. Determination of the thermodynamic parameters for CO association by ITC was impossible because the value of K^{CO} was too large (SI Figure 7).

Effects of pH on the Autoxidation of Oxy-hemoCD1. Oxy-hemoCD1 is gradually autoxidized to met-hemoCD1 in 0.05 M phosphate buffer at pH 7.0 and 25 °C under aerobic conditions. The oxidation process could be analyzed by first-order kinetics and the pseudo-first-order rate constant (k_{obs}) was determined to be 0.023 h^{-1}.[13] Similar to the autoxidation of oxy-Mb,[9] the k_{obs} value for oxy-hemoCD1 strongly depended on the pH of the aqueous solution. Figure 4 demonstrates the examples of the UV−vis spectral changes during autoxidation of oxy-hemoCD1 in aqueous solution at pH 1.95, 7.0, and 13.30 under air-saturated conditions at 25 °C. In both acidic and alkaline solutions, oxy-hemoCD1 was oxidized rapidly. The product after autoxidation was the met-hemoCD, whose iron(III) center was coordinated by H_2O at pH 1.95 or OH^- at pH 7.0 and 13.30. The pH-dependent axial ligation of met-hemoCD1 was studied previously.[20]

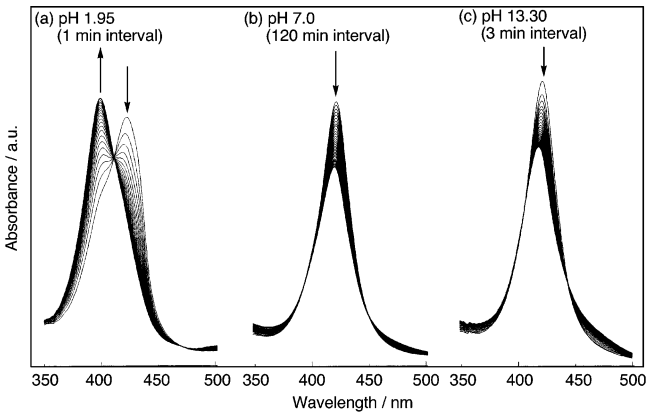

Figure 4. UV−vis spectral changes of oxy-hemoCD1 when the oxy-hemoCD1 solution was allowed to stand under aerobic conditions in aqueous solution at pH 1.95 (a), 7.0 (b), and 13.30 (c) at 25 °C. The pH values were adjusted by $HClO_4$ (a), 0.05 M phosphate buffer (b), and NaOH (c), respectively. The spectra were recorded at time intervals of 1 min (a), 120 min (b), and 3 min (c).

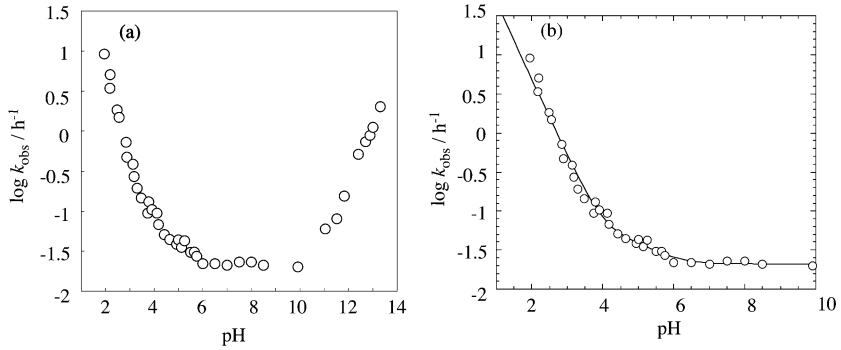

Figure 5. Plot of log(k_{obs}) versus pH for autoxidation of oxy-hemoCD1 at 25 °C (a) and curve fitting analysis for the pH-rate profile using eq 11 (b). Phosphate buffer was used for adjusting pHs between 5.0 and 8.5. The pH values between 1.95 and 5.13 and 9.91 and 13.30 were adjusted by $HClO_4$ and NaOH, respectively.

Scheme 1. pH-Dependent Autoxidation of Oxy-hemoCD1

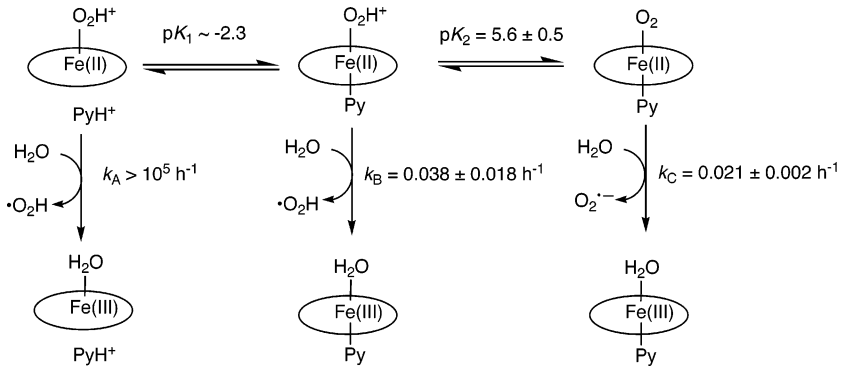

The pH−rate profile for the autoxidation of oxy-hemoCD1 is shown in Figure 5a. At pH > 10.5, the k_{obs} value increases linearly with increasing pH, indicating that the hydroxide anion attacks oxy-hemoCD1 to promote the autoxidation reaction of oxy-hemoCD1.

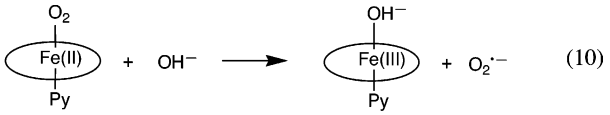

(10)

At 6.0 < pH < 10.5, oxy-hemoCD1 was very stable ($t_{1/2}$ = ca. 30 h), and the k_{obs} value was independent of pH. At 3.5 < pH < 6.0, the k_{obs} value increased with decreasing pH. Under more acidic conditions (pH < 3.5), the autoxidation was further accelerated. In acidic solution, protonation to the axial ligand occurs resulting in scission of the Fe^{III}−pyridine coordination bond. The plausible autoxidation processes of oxy-hemoCD1 in aqueous media at pH < 10.5 are shown in Scheme 1.

In Scheme 1, the water molecule is assumed to be the nucleophile that induces autoxidation. k_{obs} is represented as

$$k_{obs} = \alpha k_A + \beta k_B + (1 - \alpha - \beta)k_C \qquad (11)$$

where

$$\alpha = [H^+]^2/\{[H^+]^2 + K_1[H^+] + K_1K_2\} \qquad (12)$$

$$\beta = K_1[H^+]/\{[H^+]^2 + K_1[H^+] + K_1K_2\} \qquad (13)$$

The experimentally obtained pH−rate profile shown in Figure 5a was analyzed by eq 11 using a nonlinear least-squares method. The results are shown in Scheme 1. The curve fitting of the data for the region at pH < 3.0 must involve large errors because of the absence of saturation in the pH−rate profile (Figure 5) that causes the difficulty in determination of K_1. From the pH titration experiments, we previously confirmed that protonation to the pyridine nitrogen of **1** complexed with Zn^{II}TPPS or Fe^{III}-TPPS occurs in acidic solution at pH below 3.[20] The equilibrium between oxy-hemoCD1 and protonated oxy-hemoCD1 ($Fe^{II}-O_2H^+$) seems to account for the observed pK_2 value. The present model system is so simple that other equilibria cannot be assumed for explaining H^+-induced autoxidation in the pH range between 3.5 and 6.0. The result suggests that the $Fe^{II}-O_2H^+$ species rapidly dissociates into Fe^{III} and $\bullet O_2H$ as proposed in the biological system[30] (see Discussion).

Effect of Partial O_2 Pressure on Autoxidation. The rate of autoxidation of oxy-hemoCD1 in 0.05 M phosphate buffer at pH 7.0 and 25 °C was measured as a function of partial O_2 pressure. The O_2 partial pressures were varied from 5 to 456 Torr in N_2 atmosphere. The resulting k_{obs} values (0.018−0.025 h^{-1}) were almost constant in the range between 5 and 456 Torr (SI Figure 8). At a partial O_2 pressure of 5 Torr, only ca. 20% of hemoCD1 binds O_2, while the remaining hemoCD molecules are free. However, the k_{obs} value at 5 Torr is almost the same as that at 456 Torr. The results indicate that outer-sphere electron transfer from Fe^{II}Por to free O_2 can be eliminated from the mechanism of the

(30) Brantley, R. E., Jr.; Smerdon, S. J.; Wilkinson, A. J.; Singleton, E. W.; Olson, J. S. *J. Biol. Chem.* **1993**, *268*, 6995−7010.

Table 3. Pseudo-First-order Rate Constants (k_{obs}) for Autoxidation of Oxy-hemoCD1 in 0.05 M Phosphate Buffer in the Presence of Inorganic Anions (0.1 M) at 25 °C

	10^2k_{obs} (h^{-1})	
anion	pH 5.0	pH 7.0
none	4.5 ± 0.5	2.3 ± 0.2
N_3^-	430 ± 20	108 ± 6
OCN^-	51 ± 4	9.3 ± 3
SCN^-	6.3 ± 0.9	2.6 ± 0.4
F^-	5.2 ± 0.5	4.0 ± 0.4
Cl^-	6.0 ± 0.5	2.8 ± 0.4

Table 4. Binding Constants (K) for Coordination of Anions to Met-hemoCD1 in 0.05 M Phosphate Buffer at 25 °C[a]

	K (M^{-1})	
anion	pH 5.0	pH 7.0
N_3^-	9540 ± 164	627 ± 17
OCN^-	1890 ± 50	138 ± 8
SCN^-	53 ± 1	nd[b]
F^-	106 ± 3	nd[b]
Cl^-	11 ± 1	nd[b]

[a] The K values were determined by UV−vis spectroscopic titrations as described in ref 14. [b] nd = not determined.

autoxidation of oxy-hemoCD1 in the partial O_2 pressure range examined in this study.

Anion-Induced Autoxidation. The effects of inorganic anions on the autoxidation of oxy-hemoCD1 were investigated. The autoxidation reactions of oxy-hemoCD1 were monitored in the presence of various inorganic anions in 0.05 M phosphate buffer at pH 7.0 and 25 °C. In the presence of 0.1 M NaN_3, the considerably fast autoxidation of oxy-hemoCD1 took place in aqueous solution (SI Figure 9). The absorption band at 365 nm, which gradually increased as the autoxidation of oxy-hemoCD1 in the presence of NaN_3, indicated that the final product of the autoxidation is the N_3^--coordinated met-hemoCD1 (the UV−vis spectrum of N_3^--coordinated met-hemoCD1 is shown in SI Figure 10). All UV−vis spectral changes for the autoxidation of oxy-hemoCD1 in the presence of various anions showed the clear isosbestic points, and all reactions followed first-order kinetics (SI Figure 11). The pseudo-first-order rate constants are shown in Table 3, which shows the large acceleration effects of N_3^- and OCN^- and the weak effect of SCN^-, F^-, and Cl^- on the autoxidation of oxy-hemoCD1. The effects of the inorganic anions are correlated with the stabilities of the anion-coordinated met-hemoCD1. Each binding constant (K) for coordination of an anion to met-hemoCD1 was determined from the curve fitting analysis of the UV−vis spectroscopic titration (SI Figures 10, 12−15). Table 4 shows the K values in 0.05 M phosphate buffer solutions at pH 7.0 and 5.0. A comparison of the results in Table 4 with those in Table 3 shows that the anion with the large K value causes the rapid autoxidation of oxy-hemoCD1. The anion-coordinated met-hemoCD1s were the final products.

The k_{obs} values for the autoxidation increased linearly with increasing the concentrations of N_3^- and OH^- (Figure 6). The results clearly indicate that the nucleophilic attack of the anions on oxy-hemoCD1 is the rate-determining step. The second-order rate constants (k_X) for the autoxidation catalyzed by N_3^- and OH^- at various temperatures were

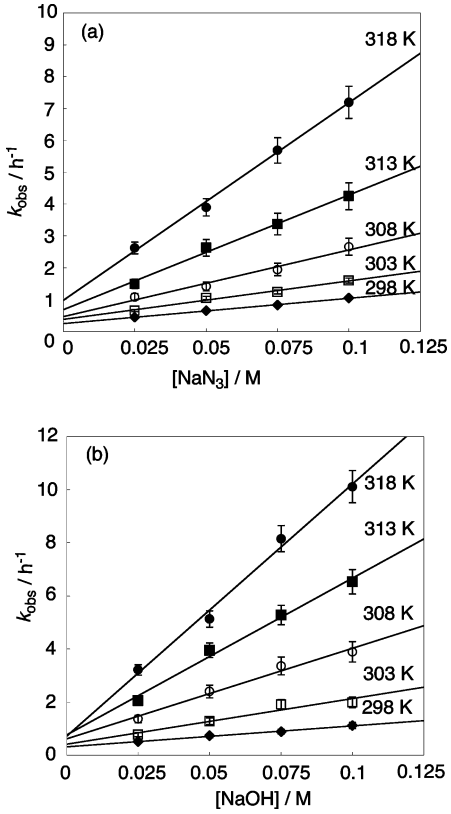

Figure 6. Plots of k_{obs} for autoxidation of oxy-hemoCD1 versus [NaN_3] in 0.05 M phosphate buffer at pH 7.0 (a) and [NaOH] in water (b) at various temperatures. The second-order rate constants (k_X) were determined from the slopes of these regression lines.

Table 5. Second-order Rate Constants (k_X) for Autoxidation of Oxy-hemoCD1 Catalyzed by Nucleophiles

	k_X (M^{-1} h^{-1})				
nucleophile	298 K	303 K	308 K	313 K	318 K
H_2O	4.1×10^{-4}	8.3×10^{-4}	1.6×10^{-3}	2.9×10^{-3}	5.2×10^{-3}
N_3^-	7.3	12.1	20.9	36.0	62.0
OH^-	8.6	17.2	34.1	59.8	95.0

Table 6. Activation Parameters for Autoxidation of Oxy-hemoCD1 Induced by Nucleophiles at 25 °C

nucleophile	$\Delta G^{\ddagger}$ (kJ mol^{-1})	$\Delta H^{\ddagger}$ (kJ mol^{-1})	$\Delta S^{\ddagger}$ (J mol^{-1} K^{-1})
H_2O	158.9	96.7	−53.0
N_3^-	88.5	83.2	−17.8
OH^-	87.8	92.8	16.7

determined from the results shown in Figure 6 (Table 5). The k_X values for the H_2O-catalyzed autoxidation were determined by dividing the k_{obs} values at the respective temperatures by the concentration of H_2O (55.5 M). The linear Eyring plots of the data in Table 5 (SI Figures 16 and 17) provided the activation free energy ($\Delta G^{\ddagger}$), enthalpy ($\Delta H^{\ddagger}$), and entropy changes ($\Delta S^{\ddagger}$) for the autoxidation of oxy-hemoCD1. The results are shown in Table 6. The $\Delta G^{\ddagger}$ values for the N_3^-- and OH^--catalyzed autoxidation reactions were ca. 1.8-fold smaller than that of the H_2O-catalyzed reaction. The effect of the anions was reflected in $\Delta S^{\ddagger}$, the $\Delta S^{\ddagger}$ values for the N_3^-- and OH^--catalyzed reactions being much larger than that for the H_2O-catalyzed reaction. The data suggest the occurrence of dehydration from the N_3^- or OH^- anion in the transition state of the autoxidation process.

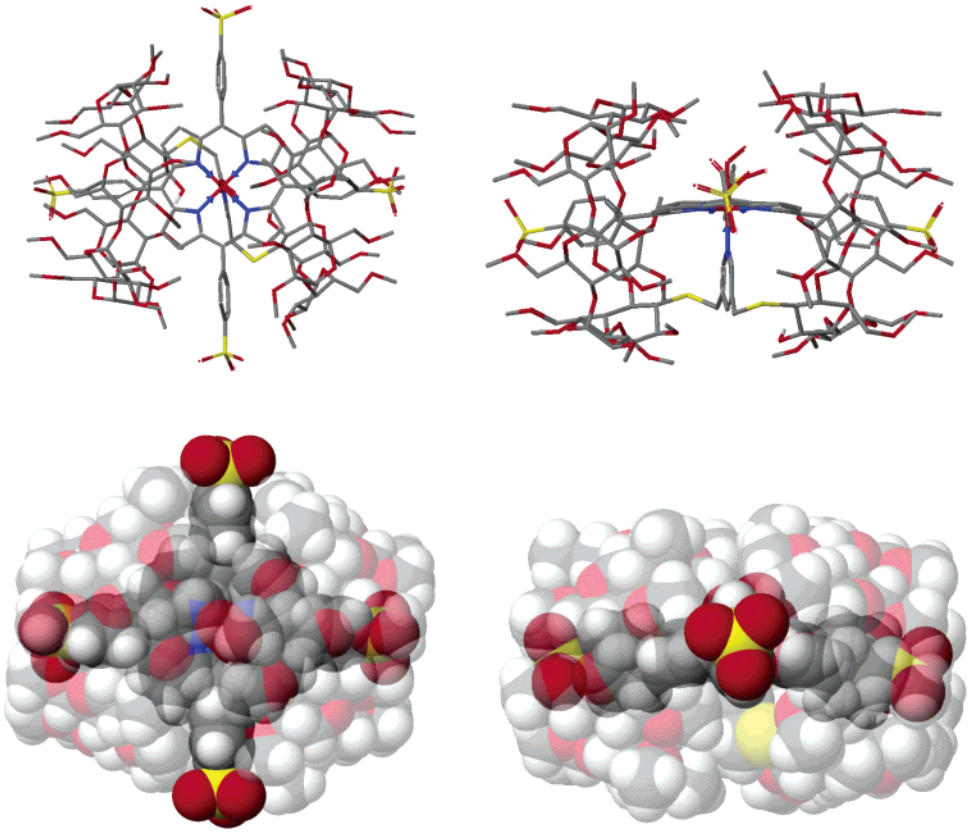

Figure 7. Energy-minimized structures of oxy-hemoCD1 obtained from the MM2 calculations using a BioMedCAChe 6.0. In the stick models (upper), the hydrogen atoms are omitted for clarity. The contribution of the solvent was neglected.

Discussion

Mb Functional Model Systems in Aqueous Solution. HemoCD1 is a unique Mb (Hb) functional model that binds dioxygen reversibly in aqueous solution.[13] Although several attempts were carried out to prepare Mb or Hb models that work in aqueous solution,[4−6] no formation of stable O_2 adducts was reported except for the cases where hydrophobic Fe^{II}Pors were placed in very hydrophobic liposomal membranes or albumin.[10,12] Recently, Zhou and Groves reported a Mb functional model composed of a water-soluble FePor and a cyclodextrin with hydrophobic tails and a tail with a base.[31] Although they observed UV−vis spectra similar to those of the O_2 and CO adducts of the Fe^{II}Por in aqueous solution, no other evidence supporting formation of the O_2 adduct has been presented. In comparison to these previous model systems, hemoCD1 shows striking behavior in aqueous solution. We deduced the structure of hemoCD1 and its derivatives.[20] The present study revealed the structure of hemoCD1 as shown in Figure 1. Further confirmation of the structure of oxy-hemoCD1 was carried out by molecular mechanics (MM) calculations. In this calculation, the contribution of the solvent was neglected. The energy-minimized structure of oxy-hemoCD1 is shown in Figure 7. The calculated structure depends on the initial structure preformed before calculation. Therefore, the structure shown in Figure 7 is one of the plausible structures. However, every calculation for various initial structures indicates the formation of finely symmetrical structures of oxy-hemoCD1, while the degree of covering of a porphyrin ring by the two cyclodextrin moieties of the dimer **1** is affected to some extent by the initial structure. In Figure 7, a porphyrin center of oxy-hemoCD1 is almost completely covered by the cyclodextrin moieties.

The novel behavior of **1** as a globin functional model can be explained by three points. First, the O-methylated β-cyclodextrin moieties of **1** include the sulfonatophenyl groups of Fe(TPPS) very tightly because of their high ability to form induced-fit type inclusion complexes.[18,19] The sulfonatophenyl groups play an important role in the preparation of the less-fluctuating inclusion complex. The hydrophilic SO_3^- group interferes with active movement of the sulfonatophenyl group as previously reported.[18] The water molecules bound to the SO_3^- groups might reduce the movement of Fe(TPPS) encapsuled by cyclodextrin cavities. Second, as demonstrated by Breslow et al.,[32] the unique property of cyclodextrin dimers in inclusion phenomena should be noticed. In general, cyclodextrin dimers tend to sandwich relatively large guest molecules to yield extremely stable 1:1 inclusion complexes. Third, dimer **1** possesses a pyridine moiety that coordinates to the iron(III) and iron(II) centers of FePors leading to fixation of the FePors in the cavities of dimer **1**. Dimer **1** has three factors required for strong inclusion of Fe(TPPS). The binding constant (K) for complexation of protoporphyrin IX with globin has been reported to be 8×10^{13} M^{-1}.[33]

(31) Zhou, H.; Groves, J. T. *Biophys. Chem.* **2003**, *105*, 639−648.

(32) Breslow, R.; Dong, S. D. *Chem. Rev.* **1998**, *98*, 1997−2011 and references therein.

Although we did not attempt to determine K for the complexation of Fe(TPPS) with **1**, the 1:1 complex (met-hemoCD1) was formed quantitatively even in an equimolar solution (4×10^{-6} M) of Fe^{III}TPPS and **1** for measuring the UV−vis spectrum.

Although hydrophobic Fe^{II}TPP was expected to be a better model, oxy-hemoCD2 was more labile than oxy-hemoCD1. Probably, the more fluctuant nature of Fe^{II}TPP in the cavities of **1** causes easier penetration of a water molecule into the cleft of oxy-hemoCD2 leading to faster autoxidation of oxy-hemoCD2. The intermolecular 2:1 inclusion complex of TMe-β-CD and Fe^{II}TPPS coordinated by 2MeIm (hemoCD3) did not form its O_2 adduct at all because of expansion of the cleft formed by two TMe-β-CD molecules caused by the bulky methyl group of 2MeIm and the much more fluctuant nature. The MM calculation supported the expansion of the cleft of hemoCD3 by the methyl group of 2MeIm.

These results suggest the essential role of the hydrophobic environment at the cleft formed by two cyclodextrin moieties of hemoCD1 to form the stable O_2 adduct of Fe^{II}Por. The cleft of hemoCD1 should be more hydrophobic than those of hemoCD2 and hemoCD3. To confirm this point, the pK_a value of free-base TPPS complexed with **1** was compared with that of the TPPS−(TMe-β-CD)$_2$ complex. In the absence of cyclodextrin, the pK_a value of TPPS is 4.8.[34] The pK_a value of TPPS dramatically decreases to 0.4 upon complexation with TMe-β-CD ([TPPS] $= 6 \times 10^{-6}$ M, [TMe-β-CD] $= 1 \times 10^{-2}$ M), indicating that two TMe-β-CD molecules provide a very hydrophobic environment at the porphyrin center. Interestingly, the cyclodextrin dimer **1** strictly inhibited the protonation to the pyrrole nitrogens of TPPS included by **1** even at pH 0.2 (SI Figure 18). It can be concluded, therefore, that the dimer **1** forms the abnormally tight inclusion complex of Fe^{II}TPPS and provides the very hydrophobic environment around the iron center of the porphyrin.

HemoCD1 does not activate O_2. No oxidized product of dimer **1** which has two oxidizable thioether groups was detected by means of FAB-MS spectroscopy after complete autoxidation of oxy-hemoCD1.

Thermodynamics of O_2 Association. To the best of our knowledge, only one example of a microcalorimetric study on the O_2 and CO association with Mb (Hb) is known.[35] The enthalpy changes ($\Delta H°$) for association of O_2 and CO with Mb (sperm whale) and Hb (human) were determined to be −67.4 and −50.6 kJ mol^{-1}, respectively, at 10−25 °C.[35c] No temperature effect on $\Delta H°$ was observed. In most previous studies, however, the thermodynamic parameters for the O_2 association with hemoproteins were determined from the modified van't Hoff plots (see eq 8). Table 2 summarizes the thermodynamic parameters reported in the references and obtained in this work. We derived $\Delta S°$ and $\Delta G°$ from the original $\Delta S'$ reported for the native and model systems by using eqs 7−9. In general, the microcalorimetric method is desirable to obtain accurate thermodynamic parameters. We applied ITC to determine the thermodynamic parameters for the O_2 association with hemoCD1 and measured the excellent titration curve that afforded $K^{O2} = (2.71 \pm 0.51) \times 10^4$ M^{-1}, $\Delta H° = -65.2 \pm 4.4$ kJ mol^{-1}, and $\Delta S° = -133.9 \pm 16.1$ J mol^{-1} K^{-1}. The K^{O2} value determined is consistent with that calculated from $P^{O2}_{1/2}$ ($(3.54 \pm 0.42) \times 10^4$ M^{-1}) using eq 7. Dioxygen association with hemoCD1 is an enthalpically favorable but entropically unfavorable process as in the biological systems. A detailed comparison of the thermodynamic data between the biological and model systems should be limited because many factors participate in the thermodynamic parameters in biological systems.

O_2−CO Selectivity. In the kinetics of ligand binding of the hemoCD1 system, we must consider two modes, binding of the ligand inside the cleft and binding of the ligand outside of the cleft. In the present study, we measured the association rates of the ligands (O_2 and CO) outside of the cleft with hemoCD1 and the dissociation rates of O_2 and CO from oxy-hemoCD1 and CO-hemoCD1, respectively, of which the ligands break out to the aqueous bulk phase. Therefore, the hemoCD1−O_2 and hemoCD1−CO pairs inside the cleft were assumed to be the same as oxy-hemoCD1 and CO-hemoCD1, respectively. The k^{O2}_{on} and k^{CO}_{on} values of Mb and Hb in Table 1 were measured by the method same as the present one, while the k^{O2}_{off} and k^{CO}_{off} values for the biological systems were evaluated from the ligand replacement reactions where released ligand could not recombine with deoxyMb or deoxyHb.[23] Consequently, the k_{off} values obtained in the present study cannot be compared directly with those for biological systems.

The smaller k^{O2}_{on} values in the biological systems may be caused by the wrapping of protoporphyrin IX in globin. The k^{O2}_{on} value for hemoCD1 is smaller than those for the picket-fence type models in toluene. The narrow cleft of hemoCD1 accounts for the slower approach of O_2 to the iron center. The much smaller k^{O2}_{off} values for biological systems are interpreted in terms of stabilization of the O_2 adducts by the distal His. Interestingly, the apparent k^{O2}_{off} value for oxy-hemoCD1 is somewhat smaller than those for the model systems in toluene.

The k^{CO}_{on} values for Mb and Hb are smaller than those for the model systems. All model systems show the k^{CO}_{on} values in the order of 10^7 M^{-1} s^{-1}, while those for Mb and Hb are 1 or 2 orders of magnitude smaller. The k^{CO}_{on} value should be affected by the spatial conditions around Fe^{II}Por.[36] An entrance to the iron center at the globin surface and a narrower space around heme in the biological system seem to lower the k^{CO}_{on} values. The problem is k^{CO}_{off}. The k^{CO}_{off} values for CO−Mb and CO−Hb are not peculiar but are somewhat smaller than those for the model systems in organic solvent.

(33) Hargrove, M. S.; Barrick, D.; Olson, J. S. *Biochemistry* **1996**, *35*, 11293−11299.
(34) Kalyanasundaram, K. *J. Chem. Soc., Faraday Trans. 2* **1983**, *79*, 1365−1374.
(35) (a) Johnson, C. R.; Angeletti, M.; Pucciarelli, S.; Freire, E. *Biophys. Chem.* **1996**, *59*, 107−117. (b) Johnson, C. R.; Ownby, D. W.; Gill, S. J.; Peters, K. S. *Biochemistry* **1992**, *31*, 10074−10082. (c) Johnson, C. R.; Gill, S. J.; Peters, K. S. *Biophys. Chem.* **1992**, *45*, 7−15. (d) Parody-Morreale, A.; Robert, C. H.; Bishop, G. A.; Gill, S. J. *J. Biol. Chem.* **1987**, *262*, 10994−10999.
(36) Collman, J. P.; Fu, L. *Acc. Chem. Res.* **1999**, *32*, 455−463.

Meanwhile, the apparent k_{off}^{CO} value for CO-hemoCD1 in aqueous solution is markedly smaller than those for CO−Mb and CO−Hb and for model systems in toluene. Olson et al. reported that disappearance of hydrogen bonding between bound CO and the distal His and an increase in polarity around the heme center shift ν_{CO} to higher frequency regions, and a positive linear correlation exists between log k_{off}^{CO} and ν_{CO} (cm^{-1}).[37] Destabilization of the CO adducts by polar effects in model systems has also been demonstrated.[26,38] A negative linear correlation was found between the ν_{Fe-CO} and ν_{CO} frequencies, and it was concluded that stronger back-bonding ($d_\pi(Fe) \rightarrow \pi^*(CO)$) causes an increase in the ν_{Fe-CO} frequency and a decrease in the ν_{CO} frequency.[39a,40] The ν_{Fe-CO} and ν_{CO} bands of CO-hemoCD1 were observed at 480 and 1987 cm^{-1}, respectively (Figure 3). The plot for the CO-hemoCD1 system lies on the right end of a straight line showing the correlation between the ν_{Fe-CO} and ν_{CO} frequencies (SI Figure 19), suggesting very weak $d_\pi(Fe) \rightarrow \pi^*(CO)$ back-bonding. The previous findings suggest that a CO adduct with weak back-bonding tends to dissociate easily.[26,37,39b] Contrary to the vibrational spectroscopic results, the k_{off}^{CO} value for the CO-hemoCD1 is the smallest among the biological and model systems in Table 1. Therefore, we need to consider another mechanism to account for the stabilization and destabilization of the CO adduct. The solubility of CO gas in organic solvent is much larger than that in water, indicating the hydrophobic nature of CO. The binding site of CO in hemoCD1 is very close to the aqueous bulk phase. There are two possible pathways for CO release, going out to the aqueous bulk phase and staying in the hydrophobic cleft of hemoCD1. The hydrophobic CO molecule must predominantly remain in the cleft of hemoCD1 with a very narrow space and then the released CO must recombine rapidly with hemoCD1. Such a process is similar to a reaction in a cage. This could account for the very small k_{off}^{CO} value and the extremely large M value (1.1×10^6) in the hemoCD1 system. The situation of CO−Mb and CO−Hb is similar to that of CO-hemoCD1. In the cases of CO−Mb and CO−Hb, however, the released CO molecule can move in the hydrophobic environments of the proteins.[41]

Autoxidation. It has been known that the autoxidation rate of oxyMb strongly depends on pH of the solution.[9,42] To discuss the effects of pH on the autoxidation in biological system, pH-dependent structural changes of the protein should be considered. Since oxy-hemoCD1 does not change its structure upon altering pH, we can discuss the autoxidation mechanism in aqueous solution without worry about the pH-dependent structural change of the environment around the iron center. In the pH range above 10.5, k_{obs} for the autoxidation of oxy-hemoCD1 increases linearly with increasing $[OH^-]$ leading to the second-order rate constant (k_X) of 8.58 M^{-1} h^{-1} at 25 °C. The results clearly indicate that the bimolecular reaction between oxy-hemoCD1 and OH^- promotes the autoxidation. Since the $\Delta S^\ddagger$ value for this reaction is positive (16.7 J $mol^{-1}K^{-1}$), dehydration from the OH^- anion seems to occur in the transition state. It can be concluded that the OH^--induced autoxidation of oxy-hemoCD1 (eq 10) takes place at a pH greater than 10.5.

The acceleration of the autoxidation in the pH range between 3.5 and 6.0 remains somewhat problematic. As shown in Scheme 1, we assumed protonation to the bound O_2 in oxy-hemoCD1 that causes the acceleration of the autoxidation. Olson et al. investigated the autoxidation rates of various oxyMb mutants as a function of pH.[30] Despite the different protein structures of the oxyMb mutants, the pH dependency for the autoxidation was essentially the same for all the proteins examined. They concluded that the acceleration of the autoxidation at lower pH is attributed to the formation of $Fe^{II}-O_2H^+$, which rapidly dissociates into the Fe^{III} and $\bullet O_2H$. The pK_a value for the equilibrium between $Fe^{II}-O_2$ and $Fe^{II}-O_2H^+$ in the hemoCD1 system was assumed to be 5.6 ± 0.5 from the curve fitting analysis of the pH−rate profile for the autoxidation of oxy-hemoCD1 (Scheme 1). Such a pK_a value for oxy-hemoCD1 is close to that for the oxyMb without distal His residue (pK_a = 6.1 for *Aplysia* oxyMb).[42c] Our results might support the mechanism of the proton-induced autoxidation in the biological system in the pH 5.0−7.0 range that was demonstrated by Olson et al.[30]

The autoxidation rate of oxyMb and oxyHb is affected by partial O_2 pressure and has the maximum value when the partial O_2 pressure is equal to $P_{1/2}^{O2}$.[43] Two types of autoxidation mechanisms competing against each other have been assumed for the biological system.[30] These are an intermolecular electron transfer from deoxyMb to free O_2 at lower $[O_2]$ (outer-sphere electron transfer) and direct dissociation of oxyMb to metMb and $O_2^{\bullet-}$ at higher $[O_2]$ (S_N1-type).[30] In contrast with the biological systems, no practical effect of dioxygen pressure on the autoxidation of oxy-hemoCD1 was observed in the range between 5 and 456 Torr (k_{obs} = 0.018−0.025 h^{-1}) in 0.05 M phosphate buffer at pH 7.0 and 25 °C. From these results, we concluded that the mechanism involving outer-sphere electron transfer from deoxy-hemoCD1 to free O_2 is negligible in the present functional model system under these partial O_2 pressures.

Anion-induced autoxidation of a heme−dioxygen complex was first observed by Wallace et al. for oxyHb.[44] Autoxidation of oxyHb is markedly accelerated by the anions such as N_3^-, SCN^-, and CN^-. The bound dioxygen of oxyHb is

(37) Li, T.; Quillin, M. L.; Phillips, G. N., Jr.; Olson, J. S. *Biochemistry* **1994**, *33*, 1433−1446.
(38) Spiro, T. G.; Kozlowski, P. M. *Acc. Chem. Res.* **2001**, *34*, 137−144.
(39) (a) Ray, G. B.; Li, X.-Y.; Ibers, J. A.; Sessler, J. L.; Spiro, T. G. *J. Am. Chem. Soc.* **1994**, *116*, 162−176. (b) Mtsu-ura, M.; Tani, F.; Naruta, Y. *J. Am. Chem. Soc.* **2002**, *124*, 1941−1950.
(40) Li, X.-Y.; Spiro, T. G. *J. Am. Chem. Soc.* **1988**, *110*, 6024−6033.
(41) Nishihara, Y.; Sakakura, M.; Kimura, Y.; Terazima, M. *J. Am. Chem. Soc.* **2004**, *126*, 11877−11888 and references therein.
(42) (a) Sugawara, Y.; Shikama, K. *Eur. J. Biochem.* **1978**, *91*, 407−413. (b) Sugawara, Y.; Shikama, K. *Eur. J. Biochem.* **1980**, *110*, 241−246. (c) Shikama, K.; Matsuoka, A. *Biochemistry* **1986**, *25*, 3898−3903.
(43) (a) Brooks, J. *Proc. R. Soc. London, Ser. B.* **1935**, *118*, 560−577. (b) George, P.; Stratmann, C. J. *Biochem. J.* **1952**, *51*, 418−425.
(44) (a) Wallace, W. J.; Maxwell, J. C.; Caughey, W. S. *Biochem. Biophys. Res. Commun.* **1974**, *57*, 1104−1110. (b) Wallace, W. J.; Houtchens, R. A.; Maxwell, J. C.; Caughey, W. S. *J. Biol. Chem.* **1982**, *257*, 4966−4977.

replaced by these anions to yield anion-bound metHb. Shikama et al. also studied the inorganic anion-induced autoxidation of oxyMb where the anions act as nucleophiles.[45] On the other hand, Olson et al. found that the pseudo-first-order rate constant for the autoxidation of oxyMb is independent of the azide concentration at pH 7.0 and 37 °C under O_2 atmosphere, even though the autoxidation rate is significantly enhanced by the N_3^- anion at lower partial O_2 pressures.[30] On the basis of the results, they proposed direct dissociation mechanism from $Fe^{II}-O_2$ to Fe^{III} and $O_2^{\bullet-}$ at higher O_2 pressure. In addition to this discrepancy, the effects of anion binding sites other than the iron center should be considered to discuss the anion-induced autoxidation of oxyMb. It was reported that coordination of the N_3^- anion to metMb is prevented by other anions such as ClO_4^-, I^-, Br^-, Cl^-, and SO_4^{2-}.[46] Since the ClO_4^- and SO_4^{2-} anions do not coordinate to metMb, anion-binding sites other than the iron center must exist in metMb. DeRosa et al. postulated a conformational change of metMb upon binding of an additional anion leading to prevention of N_3^- ligation to the Fe^{III} center.[46] The Cl^- anion is known to alter the conformation of Hb to affect the O_2 uptake.[47] These aspects suggest the difficulty in clarification of the mechanism for the anion-catalyzed autoxidation of oxy-hemes in biological systems. The present model system is so simple that the experimental results can be used directly to discuss the mechanism of the autoxidation of oxy-hemoCD1 catalyzed by inorganic anions. The results in Table 3 reveal the large acceleration effect of N_3^- and OCN^- and the weak effect of SCN^-, F^-, and Cl^- on the autoxidation of oxy-hemoCD1. The important result concerning the anion-induced autoxidation is that the autoxidation of oxy-hemoCD1 follows second-order kinetics. Such a finding clearly indicates the attack of the anion to oxy-hemoCD1 at the rate-determining step. The $\Delta S^{\ddagger}$ for the N_3^--induced autoxidation of oxy-hemoCD1 is negative, but much larger than that for the H_2O-induced autoxidation (Table 6). Dehydration from the N_3^- anion in the transition state might also occur as in the case of the OH^--induced autoxidation. In other words, the anion causes the bimolecular autoxidation of oxy-hemoCD1. We previously found that HPO_4^-, HSO_4^-, and ClO_4^- do not coordinate to the Fe^{III}TPPS-TMe-β-CD complex.[14] These inactive anions did not induce the autoxidation of oxy-hemoCD1. Taken together, the results strongly support the notion that a bimolecular mechanism is involved in the anion-induced autoxidation of oxyMb.[9,45]

Conclusions

The present study leads to the following conclusions:

(1) To prepare a stable dioxygen adduct of a ferrous porphyrin in aqueous solution, the Fe^{II} center should be placed in a stable, nonfluctuating, hydrophobic environment from which the H_2O molecule is completely excluded. These requirements are absolute. HemoCD1 meets such absolute requirements.

(2) Dissociation of CO from a CO adduct of Fe^{II}Por is markedly affected by the medium surrounding the Fe^{II} center. Hydrophobic CO released from CO-hemoCD1 hardly diffuses to the aqueous bulk phase since hemoCD1 has a very narrow, shallow, hydrophobic cleft surrounded by an aqueous bulk phase. Therefore, rebinding of CO to hemoCD1 inside the cleft easily occurs resulting in extreme stability of CO-hemoCD1.

(3) Dioxygen binding to hemoCD1 is an enthalpically favorable but entropically unfavorable process. Although this type of thermodynamic behavior is similar to that of biological Mb, a comparative discussion between the biological and model systems is difficult.

(4) Autoxidation of oxy-hemoCD1 occurs through bimolecular nucleophilic reactions where H_2O and certain anions act as nucleophiles.

Acknowledgment. This study was supported by Grants-in-Aid on Scientific Research B (No. 14340224 and 17350074) and on Scientific Research for Priority Area (No. 16041243) from the Ministry of Education, Culture, Sports, Science and Technology, Japan.

Supporting Information Available: UV−vis spectra of hemoCD2 and its O_2 and CO complexes, spectral changes of oxy-hemoCD2 during autoxidation, ^{1}H NMR spectra of the Fe^{II}TPPS−TMe-β-CD complex in D_2O in the absence and presence of 2MeIm, the time courses of laser flash photolysis of oxy-hemoCD1 and CO-hemoCD1, plot for determining the second-order rate constant for O_2 association with hemoCD1, ITC titration curves for O_2 and CO binding to deoxy- and oxy-hemoCD1, plot of k_{obs} versus partial O_2 pressure, spectral changes of oxy-hemoCD1 during anion-induced autoxidation, plots for determining the pseudo-first-order rate constants for anion-induced autoxidation of oxy-hemoCD1, UV−vis spectral changes of met-hemoCD1 as a function of [anion], Eyring plots for autoxidation of oxy-hemoCD1, pH titration of TPPS-**1** complex, plot of ν_{Fe-CO} versus ν_{C-O} frequencies for CO-hemoCD1. This material is available free of charge via the Internet at http://pubs.acs.org.

IC060137B

(45) Satoh, Y.; Shikama, K. *J. Biol. Chem.* **1981**, *256*, 10272−10275.
(46) De Rosa, M. C.; Bertonati, C.; Giardina, B.; Di Stasio, E.; Brancaccio, A. *Biochim. Biophys. Acta* **2002**, *1594*, 341−352.
(47) Matra, M.; Patamia, M.; Colella, A.; Sacchi, S.; Pomponi, M.; Kovacs, K. M.; Lydersen, C.; Giardina, B. *Biochemistry* **1998**, *37*, 14024−14029.